THE ROYAL SOCIETY

Large metal clusters and lattices with analogues to biology

By Daniel J. Price[1], Frederic Lionti[2], Rafik Ballou[2], Paul T. Wood[1] and Annie K. Powell[1]†

[1]*School of Chemical Sciences, University of East Anglia, Norwich NR4 7TJ, UK*
[2]*Laboratoire Louis Néel, CNRS, 25 Avenue des Martyrs BP166, 38042 Grenoble Cedex 9, France*

The magnetic properties of two types of material derived from the brucite lattice, $M(OH)_2$ are described. The structure-directing effects of simple templates on the brucite lattice parallels the processes seen in nature in formation of biominerals. The first type exemplified by Fe_{17}/Fe_{19} aggregates models the structural features of the iron storage protein ferritin. The magnetic behaviour also reveals some interesting parallels with the magnetic phenomena reported previously on ferritins. We have used a combination of experimental techniques including DC, AC and RF susceptibility measurements on powders and a microSQUID on single crystals. The second type is based on an extended-defect brucite structure with stoichiometry $M_2(OH)_2(ox)$ for $M = Fe^{2+}$, Co^{2+}. They show long-range ordering to antiferromagnetic phases and then, at much lower temperatures, undergo a phase transition to canted antiferromagnetic states. Symmetry arguments are used to predict the spin configurations in these extended materials.

Keywords: magnetism; biominerals; clusters; hydrothermal synthesis; coordination chemistry

1. Introduction

The oxide, oxyhydroxide and hydroxide phases of paramagnetic transition-metal ions can display a variety of cooperative magnetic phenomena, such as ferromagnetism, ferrimagnetism and spin-canted antiferromagnetism, which are often useful in technological applications. The iron-containing phases prove to be particularly versatile and the chemistry and physical properties of these materials are relatively well understood (Cornell & Schwertmann 1996). The hydrolysis of iron(III) is the starting point for the formation of all the iron oxides, oxyhydroxides and hydroxides (Cornell & Schwertmann 1996; Wells 1962). In recognition of the fact that biological systems are able to manipulate the phase and form of such iron minerals (Frankel & Blakemore 1990), we have been exploring ways to achieve similar control *in vitro* by modifying the natural hydrolysis of iron(III) ions. The mineral products of iron hydrolysis adopt structures based on cubic and hexagonal lattices, but the two types can be interchanged relatively easily (Wells 1962). The initial products of both iron(III) and iron(II) hydrolysis are best described as materials adopting

† Present address: Institut für Anorganische Chemie, Universität Karlsruhe, Engesserstr. Geb. 30.45, D76128 Karlsruhe, Germany.

$$\{\mathrm{FeL}_m\}^{\pm q} + \mathrm{xs\,H_2O} \rightleftharpoons \{\mathrm{Fe}_x\mathrm{L}_n(\mathrm{O})_y(\mathrm{OH})_z(\mathrm{H_2O})_p\}^{\pm a} \rightleftharpoons \text{`Fe(OH)}_3\text{'}.$$

Scheme 1.

structures based on hexagonal close packing. In the case of iron(II), $Fe(OH)_2$ forms initially, which has the brucite structure (typified by brucite, $Mg(OH)_2$), whereas for iron(III), the more poorly defined mineral ferrihydrite is the first identifiable phase, which can be formulated in various ways and is often denoted simply by '$Fe(OH)_3$'. The formulation of this as $\{(Fe_2O_3)(2Fe\cdot O\cdot OH)(2.6H_2O)\}$ (Russell 1979) underlines the observation that the mineral is most likely to have a defect hexagonal close packed structure (Cornell & Schwertmann 1996; Towe & Bradley 1967) related to the better-defined hexagonal close packed oxyhydroxide, goethite, α-$Fe\cdot O\cdot OH$, and oxide, haematite, α-Fe_2O_3, which are the phases ferrihydrite evolves into on ageing (Cornell & Schwertmann 1996; Wells 1962). Ferrihydrite phases are often nanoparticulate, further complicating their characterization. In our research to date, we have found that modification of iron hydrolysis leads to materials based on these hexagonal close-packed (HCP) structures. It is, therefore, helpful to describe how the structures of the three well-defined phases brucite, goethite and haematite are related.

The brucite structure, $M(OH)_2$, adopts an AX_2 HCP structure related to CdI_2. It has a two-dimensional layer structure with hexagonally close packed oxygen atoms as double strips of OH^- with M(II) in octahedral holes. The hydroxide ions bridge across three metal centres. In three dimensions the layers stack up to optimize hydrogen bonding between the layers. The related structure adopted by M(III) ions, typified by goethite, is also an AX_2 structure, but, in order to preserve charge balance, there is only half the number of protons in the stoichiometry: $M\cdot O\cdot OH$. The oxygen atoms are again in an HCP arrangement with M(III) in octahedral holes, but now the protons are shared between layers in the three-dimensional structure such that the compound could also be formulated as '$M(OH_{0.5})_2$'. The oxide structure exemplified by haematite, α-Fe_2O_3, is an A_2X_3 structure, again with HCP oxygen atoms and M(III) in octahedral holes. The oxides bridge between four metal centres, the relationship to the layer structures of brucite and goethite being that a μ_4-O connects three metal ions from one layer to one in the next layer up, and so on, to give a truly three-dimensional network.

In this article we describe the structures and magnetic properties of three materials synthesized by us which can be regarded as resulting from hydrolysis reactions of transition-metal ions that have been modified by the presence of templating species and control over crystallization conditions to produce engineered metal hydroxide frameworks. The synthetic strategy is to provide a templating species, L, which enters the coordination sphere of the metal ion and in some way affects the nature of the resulting hydrolysis product, through the production of an intermediate material $\{M_xL_n(O)_y(OH)_z(H_2O)_p\}^{\pm a}$, as indicated for iron(III) in scheme 1.

It is believed that this is one of the ways in which biology is able to tailor mineral species for specific functions through the process of biomineralization (Mann *et al.* 1989). We have therefore been exploring analogous interactions *in vitro* in order to produce new materials with tailored properties.

The intermediate species $M_xL_n(O)_y(OH)_z(H_2O)_p\}^{\pm a}$ may have zero values for some of the components, but must have some oxygen atoms derived from coordinated water molecules present. The compounds we describe here can be under-

stood in terms of this intermediate material and derived from the brucite mineral structure. Firstly, we describe the situation where chelating ligands, L, can be used to encapsulate portions of the $M(OH)_2$ framework giving particles with large boundary effects and unusual magnetic properties that result from these. In general, these particles can be described in terms of $\{Fe_xL_n(O)_y(OH)_z(H_2O)_p\}^{\pm a}$, where the parameters x, n, y, z and p all have fairly small finite values, as in the case of $\{Fe_{19}L_{10}(O)_6(OH)_{14}(H_2O)_{12}\}^+$, where $L = N(CH_2COO)_2(CH_2CH_2O)^{3-}$ (see, for example, Heath & Powell 1992). Secondly, we describe the situation where the ligand, L, becomes incorporated into the brucite lattice to give a modified structure that can be regarded as a 'defect' brucite network. These extended phases can also be related to the $\{M_xL_n(O)_y(OH)_z(H_2O)_p\}^{\pm a}$ formulation, but now the overall structures are infinite and the stoichiometries are correspondingly simpler, as in the case of $\{Fe_2(L)(OH)_2\}$ where $L = C_2O_4^{2-}$ (Molinier *et al.* 1997). The lowering of the overall symmetry of the brucite lattice through these inclusions results in materials that display spin-canting phenomena.

2. Experimental

The Fe_{19} and Fe_{17} aggregates were synthesized under ambient conditions as described previously (Heath & Powell 1992; Powell *et al.* 1995). Diiron(II) dihydroxyoxalate was synthesized under hydrothermal conditions as described previously (Molinier *et al.* 1997). The sample was ground and a bar magnet was used to remove most of the ferrimagnetic magnetite impurity. Dicobalt(II) dihydroxyoxalate was also synthesized hydrothermally. A fresh cobalt hydroxide precipitate was formed by the addition of NaOH to an aqueous solution of $CoCl_2$. To this, $Na_2C_2O_4$ was added and the reaction heated to 220 °C for 2 days (Gutschke *et al.* 1999*a*).

Magnetic measurements were performed on a Quantum Design MPMS SQUID magnetometer. A few mg of each of the powdered samples were pressed into a gelatine capsule mounted onto a polyethylene straw. Field-cooled magnetization measurements were performed in longitudinally applied fields of 100 and 1000 G, over a temperature range of 2–300 K. The contribution of magnetite impurities to the iron-containing sample could not be deconvoluted, limiting the quantitative usefulness of these data. However, no such problem was encountered with the cobalt analogue. For this sample, a correction for the diamagnetic contribution to the susceptibility of -73×10^{-6} cm^3 mol^{-1} was calculated from Pascal's constants (see, for example, Kahn 1993) was applied.

The static and dynamic magnetic behaviour of the Fe_{19} and Fe_{17} aggregates were investigated in more detail at Grenoble on powdered samples using home-built AC-susceptometers and RF SQUID magnetometers equipped with dilution fridges and on a small single crystal using microSQUID devices (Wernsdorfer 1996). The real and imaginary parts of the longitudinal AC-susceptibility were measured on the powdered samples at frequencies as low as 0.005 Hz and up to 12.5 kHz in a temperature range from 50 mK up to 40 K. Some AC-susceptibility measurements were performed by superposing a static magnetic field up to 1.5 T on the weak alternating magnetic field (0.1 mT). Magnetization measurements on powdered samples could be extended to temperatures as low as 50 mK and in a range of applied magnetic fields from -5 T to 5 T. Some magnetic relaxation measurements on powdered samples were also performed. More relevant, however, were the magnetic relaxation measurements

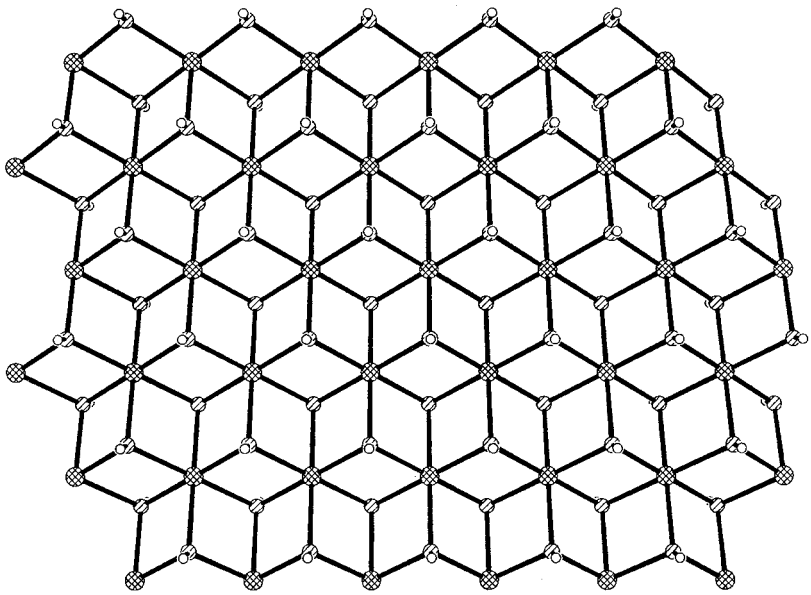

Figure 1. The layer structure of brucite showing metal ions held together in a regular triangular lattice by μ_3 bridging hydroxides.

performed on the single crystal using the microSQUID devices. For these, the applied magnetic field is limited to about 1 T but can be applied in any direction of space and, in particular, measurements can be performed under a main longitudinal field with a small transverse component. Moreover, the magnetic-field strength can be varied at a high time rate and the magnetization can be recorded with a high resolution in time, allowing clean and efficient protocols for the magnetic relaxation measurements. Working with a dilution fridge, the microSQUID data were collected within the temperature range from 30 mK to 5 K.

3. Results and discussion

(*a*) *Materials containing trapped finite portions of the brucite lattice*

Although we have been able to obtain a variety of species of general formula

$$\{M_xL_n(O)_y(OH)_z(H_2O)_p\}^{\pm a}$$

for M = Fe(III), Al(III) using the general synthetic method outlined above (Heath 1992; Womack 1999; Heath *et al.* 1995; Baissa *et al.* 1999), the most extensively studied material in terms of its magnetic behaviour is the solid formed with the ligand hydroxyethyliminodiacetic acid, $N(CH_2COOH)_2(CH_2CH_2OH) = H_3$heidi, which contains interpenetrating lattices of aggregates of 19

$$\{Fe_{19}L_{10}(O)_6(OH)_{14}(H_2O)_{12}\}^{+},$$

and 17

$$\{Fe_{17}L_8(O)_4(OH)_{16}(H_2O)_{12}\}^{3+},$$

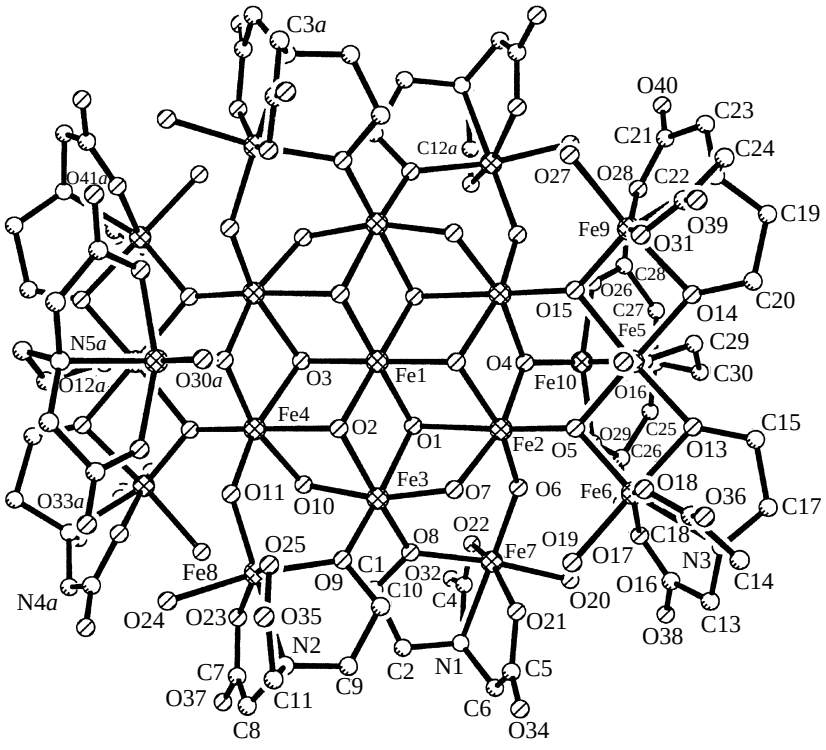

Figure 2. The molecular structure of the Fe_{19} aggregate.

iron(III) centres (Heath & Powell 1992; Powell *et al.* 1995). The fact that the two aggregates co-crystallize complicates the interpretation of the bulk magnetism, but initial magnetic studies on this material indicated that the aggregates could be regarded as particles stabilizing high ground state spins with at least one of the clusters carrying a spin in the region of 33/2 (Powell *et al.* 1995). Since this material has been structurally characterized using single-crystal X-ray diffraction we were able to suggest possible pathways for the stabilization of the high ground-state spin. The aggregates both contain cores corresponding to a brucite lattice, except, of course, the metal is in the +3 oxidation state, $\{M(OH)_2\}^+$. This can readily be seen by comparing the brucite lattice (figure 1) with the structure of the Fe_{19} aggregate (figure 2). The encapsulating peripheral iron oxide, hydroxide and ligand units serve to compensate for the build-up of positive charge on the core to give aggregates carrying rather small overall charges. This, in turn, creates a situation rather like that seen in the iron storage protein ferritin (figure 3), where an iron mineral akin to ferrihydrite is encapsulated in a shell of nucleating iron centres and protein ligands (Ford *et al.* 1984). We have shown previously that these smaller aggregates make excellent 'scale models' for loaded ferritin (Heath *et al.* 1996; Powell 1997). The structural parallels between loaded ferritin and the cluster models seem to carry over into the types of magnetic behaviour observed. It is reasonable to expect a finite aggregate to display strong boundary effects, particularly when the particle size falls within the nanoscale regime. These can be understood in terms of large surface effects giving rise to uncompensated spins (Le Brun

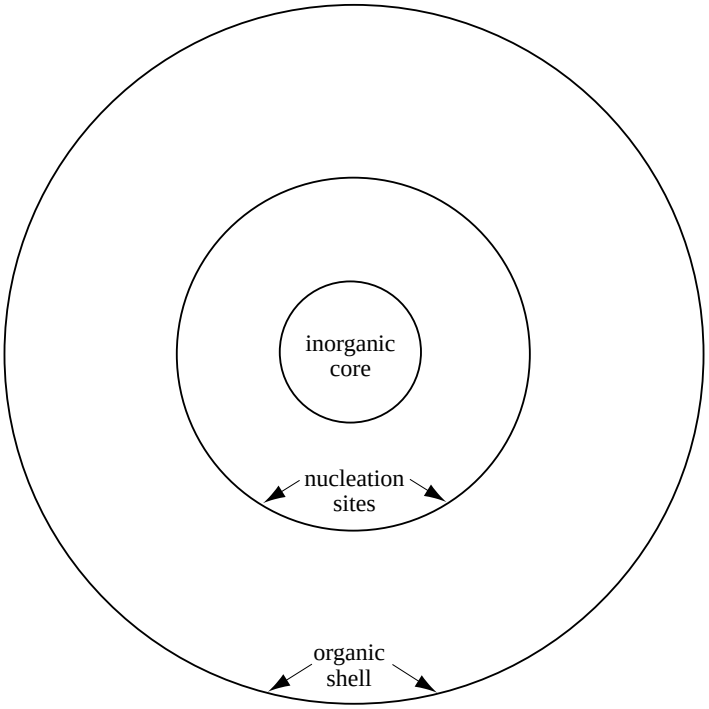

Figure 3. Representation of the structural elements of loaded ferritins.

et al. 1997, and references therein; Tejada & Zhang 1994). In the case of the Fe_{19} and Fe_{17} aggregates it is possible to propose models to explain the observed spin states. These allow for the fact that the exchange pathways amongst the iron(III) centres are different in different regions of the aggregate, also as a consequence of the boundary around the particle. In this vein, it is interesting to compare some recent ultra-low-temperature magnetic results obtained on the Fe_{19}/Fe_{17} system with some of the magnetic properties reported on both superparamagnetic molecular particles, such as $[Mn_{12}O_{12}(CH_3COO)_{16}(H_2O)_4] \cdot 2CH_3COOH \cdot 4H_2O$, commonly abbreviated to $Mn_{12}Ac$, and loaded ferritins. The former can be understood in terms of anisotropic 'single molecule magnets' of $S = 10$ displaying resonant quantum tunnelling effects (Thomas *et al.* 1996; Friedman *et al.* 1996), while the latter are examples of polydisperse systems, and, thus, the magnetic data are correspondingly harder to interpret (Awschalom *et al.* 1992). The possibility that these types of materials can be used in applications such as information storage and in quantum computing, for example, in addition to shedding light on the fundamental questions regarding the link between the molecular and the infinite, and the boundary between the quantum and macroscopic worlds, has been pointed out by several commentators (Chudvonsky 1996; Stamp 1996; Gatteschi *et al.* 1994).

The observation that $Mn_{12}Ac$ displays stepped hysteresis phenomena at temperatures where the molecules are expected to be in their ground state with a total spin per molecule of $S = 10$ has been explained in terms of resonant tunnelling between intermediate levels. Further experiments on orientated single crystals using AC susceptibility measurements (Thomas *et al.* 1996; Friedman *et al.* 1996) and also

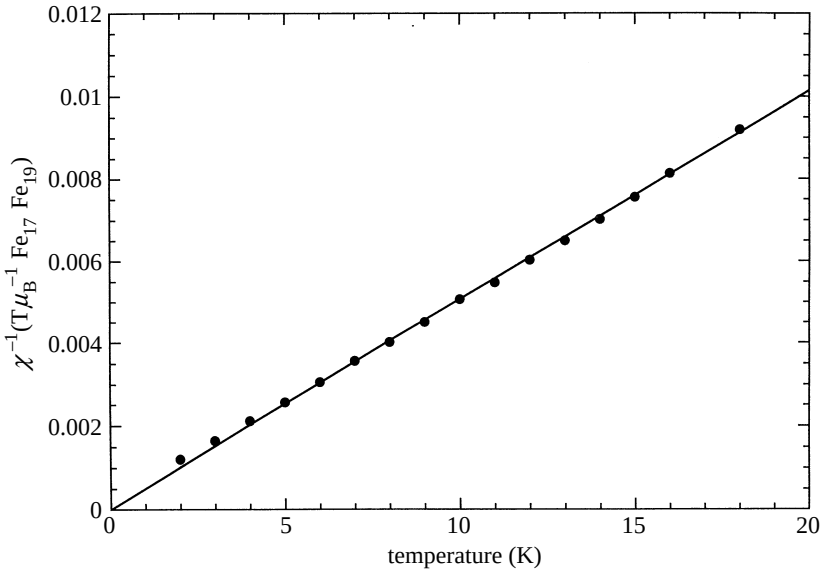

Figure 4. Plot of reciprocal susceptibility versus temperature for a powdered sample of Fe_{17}/Fe_{19} showing Curie behaviour between 5 and 18 K.

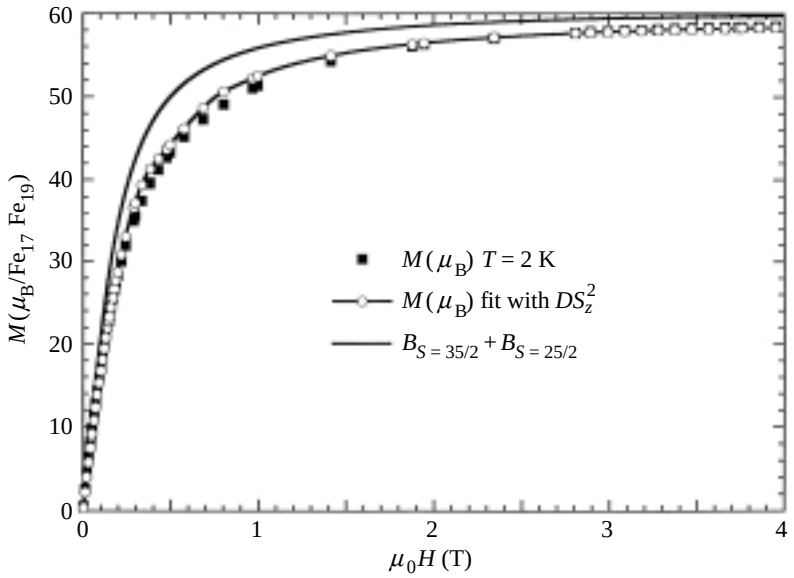

Figure 5. Magnetization isotherm at 2 K for a powdered sample of Fe_{17}/Fe_{19} (filled squares). The upper curve shows the Brillouin function for two spins of $S_1 = 35/2$ and $S_2 = 25/2$, the lower curve, with open circles, corresponds to the fit incorporating an anisotropic energy barrier.

MCD experiments on powders are in line with the bistability of this system and its superparamagnetic behaviour (Cheesman *et al.* 1997). Although there is still much debate regarding the underlying physics of these phenomena, the system itself represents a well-behaved vehicle for investigation, since it forms what can be regarded

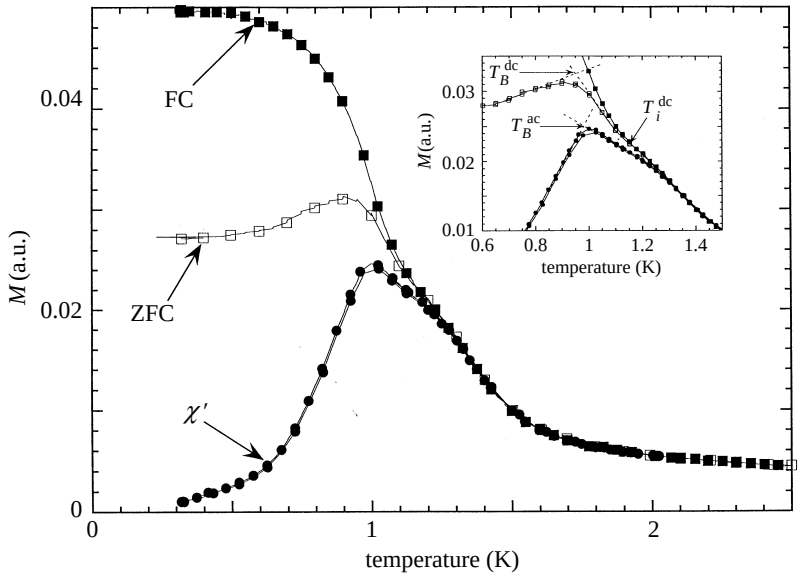

Figure 6. Thermal variation of the real part of the AC-susceptibility, zero-field-cooled and field-cooled magnetizations measured on a powdered sample of Fe_{17}/Fe_{19} showing the double-blocking behaviour.

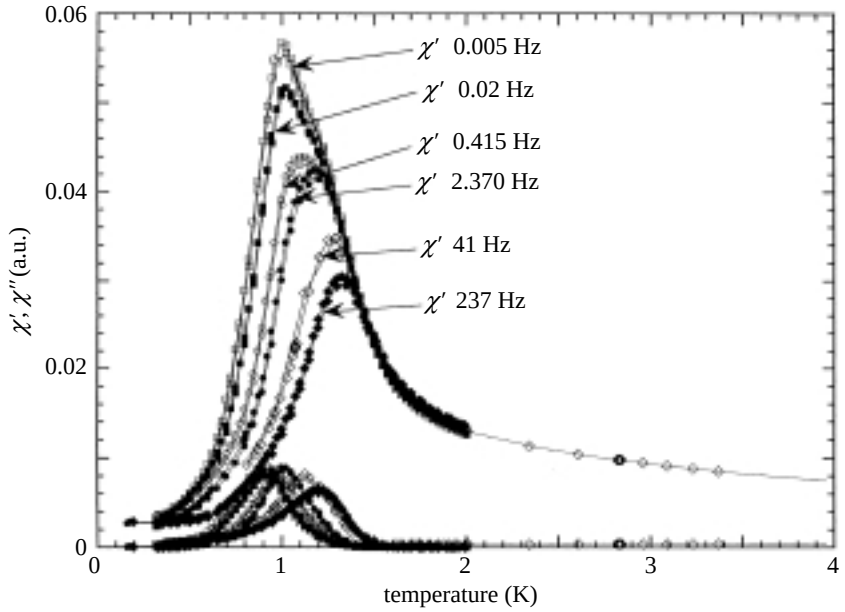

Figure 7. Thermal variation of the real and imaginary components of the AC susceptibility in the region of the blocking temperature for various driving frequencies measured on a powdered sample of Fe_{17}/Fe_{19}.

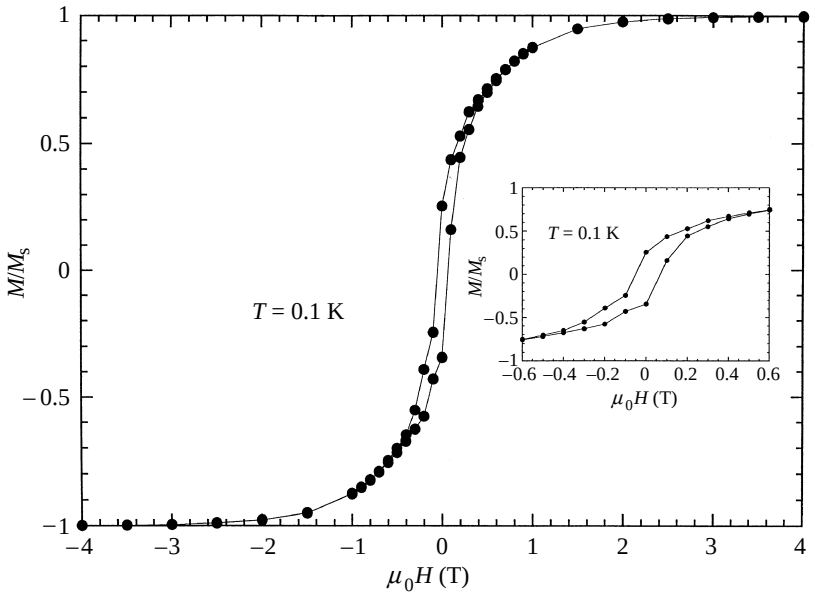

Figure 8. The magnetization isotherm of a powdered sample of Fe_{17}/Fe_{19} at 0.1 K showing a weak hysteresis.

as monodisperse highly orientated particles within a well-ordered crystal lattice with a readily identifiable easy axis of magnetization. On the other hand, materials such as loaded ferritin molecules are much harder to study. On average, a loaded ferritin molecule could contain about 4000 iron(III) centres (Ford *et al.* 1984), and the dimensions of the iron oxyhydroxide cores of these molecules correspond to spherical particles about 7 or 8 nm in diameter. Magnetic measurements such as Mössbauer spectroscopy have revealed that loaded ferritins from mammalian sources display superparamagnetism with blocking temperatures as high as 60 K. There is also evidence that such molecules display hysteresis phenomena and, from susceptibility measurements, that there could be resonant tunnelling in operation as well (Awschalom *et al.* 1992; Tejada *et al.* 1996). However, the situation here is very different from that in the $Mn_{12}Ac$ system. Although the description of both as superparamagnetic is reasonable, in the case of the loaded ferritins it becomes impossible to assign a single large spin to each molecule. Indeed, it might even be the case that, within the protein shell of a given ferritin, there are several particles occupying the 7–8 nm cavity, complicating matters even further. In any case, assuming, for simplification, that each ferritin contains a single 7–8 nm diameter particle, we can only proceed by assigning an average overall spin to the system; in other words, we are dealing with a polydisperse material.

The Fe_{17}/Fe_{19} system we describe here lies between these two examples. While the detailed molecular and crystal structure of the compound is known, as in the case of $Mn_{12}Ac$, the situation is complicated by the fact that there are two different clusters, the least-squares planes of the iron oxyhydroxide cores of which are orientated at 28° to each other. This can thus be regarded as a system in which orientation can be achieved using single crystals, but it is not as simple as in the $Mn_{12}Ac$ case since there are two sets of magnetically distinct molecules that are likely to carry different

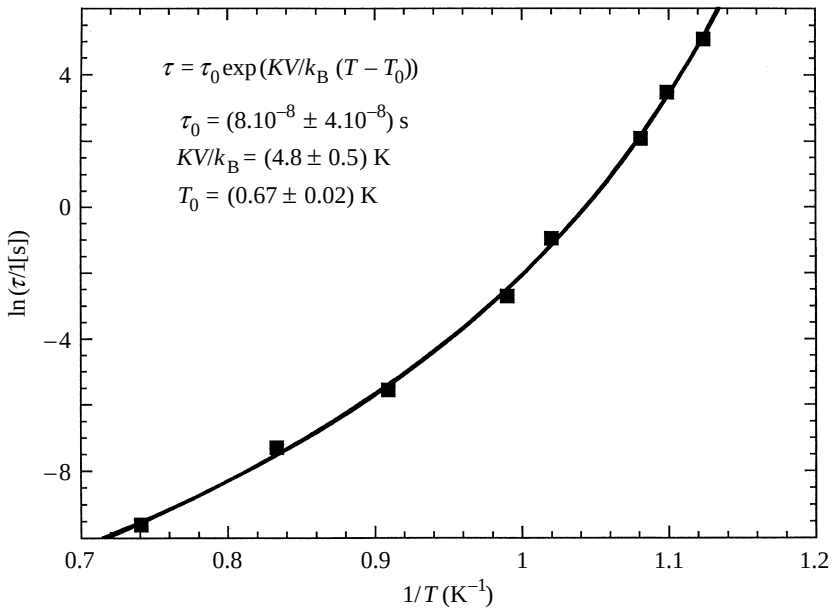

Figure 9. Logarithm of the characteristic fluctuation time of S_1 and S_2 versus inverse temperature for a powdered sample of Fe_{17}/Fe_{19}. The non-Arrhenius behaviour is indicative of a weak intercluster interaction.

total spin values and for which the easy axis of magnetization is likely to lie along different vectors for each type of aggregate.

We have found that, at very low temperatures, this material displays hysteresis phenomena that bear resemblance to the reported data for loaded ferritin cores (Awschalom *et al.* 1992; Tejada *et al.* 1996). We do not yet fully understand the physical origins of the effects that we have measured, but we can propose some possible interpretations of the data, which could give some insight into the phenomena observed for loaded ferritins.

From our new data measured on both powdered samples and orientated single crystals, we find that the system can be described as containing two magnetically distinct clusters, one of spin 25/2 and the other of spin 35/2. This conclusion is drawn from the graph of reciprocal DC susceptibility versus temperature, which obeys a Curie law over the range 4–18 K fitted for a Curie constant, C, of $C = g^2[S_1(S_1+1)+S_2(S_2+1)]$, giving an excellent fit for $g = 2.00$, $S_1 = 35/2$, $S_2 = 25/2$ (figure 4). This is supported by the magnetization data with respect to B/T (B is the Brillouin function for the spin, S) between 5 and 20 K, which fits well for $B(S = 35/2)+B(S = 25/2)$. The difference in total spin for the two clusters equates to the removal or addition of two Fe(III) high-spin ions of $S = 5/2$, which fits with the difference in molecular composition between the two aggregates. Thus we can consider the system at these temperatures as comprising sets of aggregates with overall spins of 35/2 and 25/2. Below 4 K, the scaling law with respect to B/T is no longer obeyed due to the emergence of magnetocrystalline anisotropy. A fit of the curves (figure 5) gives an anisotropy barrier of 4.8 K for $S = 25/2$ and 9.4 K for $S = 35/2$. The temperature dependence of the hysteresis shows a superparamagnetic blocking of the spins around 1 K, and the thermal variation of the real and imaginary

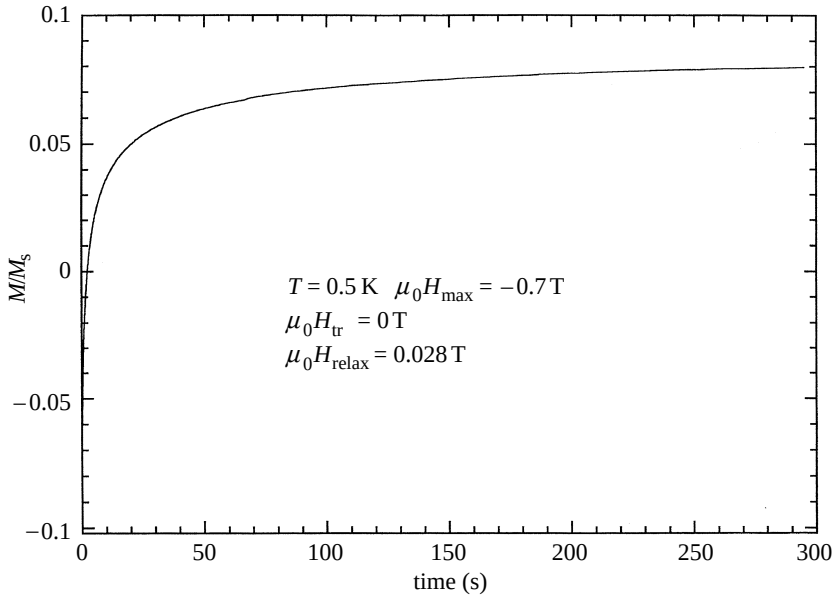

Figure 10. Temporal variation of the magnetization on a single crystal of Fe_{17}/Fe_{19} showing equilibrium magnetization, M_{eq}, is reached in about 300 s.

part of the AC susceptibility around this blocking temperature (figures 6 and 7) clearly shows a double-blocking behaviour, in agreement with the differences of the energy barriers for the two overall spins. The magnetization isotherm measured below the blocking temperature gives a weak hysteresis loop with qualitative similarities to hysteresis loops reported for loaded ferritin cores (figure 8). It is likely that there are weak intercluster interactions, as indicated by the fact that a plot of the logarithm of the fluctuation time of the spins with respect to inverse temperature does not obey an Arrhenius law (figure 9) (see, for example, Dormann *et al.* 1988). From figure 9 it can be seen that we can estimate that this interaction becomes significant at about $T = 0.67$ K.

It was also possible to measure data on a microSQUID. Since it is not possible to measure data on such an instrument on absolute scales, it is necessary to give data in terms of relative magnetization, M/M_s, where M_s is the saturation magnetization. These measurements confirmed the scaling law with respect to B/T and that this law is not obeyed below 5 K. Single-crystal studies allow relaxation phenomena to be investigated and it was found that the time to reach equilibrium of the magnetic relaxation, t_{max}, was about 300 s (figure 10). Further measurements reveal that the relaxation processes are very complex and that the measurements are difficult to interpret. The relaxation processes were investigated by measuring the variation of M_{eq}, defined as

$$M_{eq} = \tfrac{1}{2}[M(t_{max}, H_{max} \to H_{relax}) + M(t_{max}, -H_{max} \to -H_{relax})].$$

The temporal variation of $\Delta M(t)$, where $\Delta M(t) = M(t) - M_{eq}$, is more complex than is usually observed and does not follow exponential, stretched exponential or even logarithmic behaviour as shown in figure 11. A relaxation protocol was used in which the sample was initially heated from 5 K with a field of −0.7 T applied,

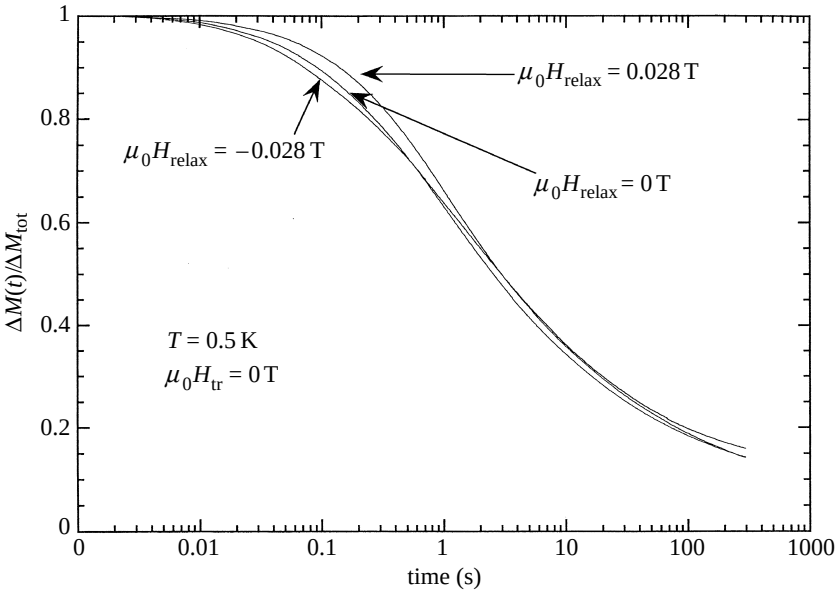

Figure 11. Temporal variation of $\Delta M(t)$ (see text) on a single crystal of Fe_{17}/Fe_{19}. The complex relaxation processes of this system are evident from the inability to fit these curves using exponential, stretched exponential or even logarithmic forms.

which aligns all the $S_1 = 35/2$ and $S_2 = 25/2$ along the field. The sample was then cooled under this field. At the given measuring temperature, the field was switched to the measuring field, H_{meas}, at a sweeping rate of 0.14 T s^{-1}. Our present analysis of the observed relaxation behaviour suggests that when H_{meas} is of the order of the molecular field, $H_{\mathrm{int}} = -0.1$ T, describing the antiferromagnetic interactions between the two spins, the applied field can no longer maintain the parallel alignment of these spins and $S_2 = 25/2$ tends to reverse its orientation by overcoming the anisotropy barrier of 4.8 K either thermally or by tunnelling. When H_{meas} is close to zero, the two spins are antiparallel and to reverse the orientation they have to overcome the sum of the two anisotropy barriers again either thermally or through tunnelling. Conversely, when H_{meas} is of the order of $H_{\mathrm{int}} = 0.1$ T, it is the spin $S_1 = 35/2$ that will tend to align parallel to the field and must overcome the associated anisotropy barrier.

Clearly, the Fe_{17}/Fe_{19} system has a much more complicated magnetic behaviour than the $Mn_{12}Ac$ system and we are still far from understanding the intricacies of the relaxation phenomena. However, comparing these results with some of those reported on ferritins, we can see that an understanding of the data we have measured could give useful insights into the physics of the polydisperse ferritin systems as well as other systems of polydisperse antiferromagnetically coupled particles.

(*b*) *Extended-defect brucite structures*

The hydrolysis of iron(III) or cobalt(II) salts followed by hydrothermal reaction conditions in the presence of the oxalate ligand leads to infinite structures incorporating the oxalate ion into a defect brucite lattice as $M_2(OH)_2(ox)$. As we have reported previously, in the case of iron(III), this reaction results in the stabilization of iron(II), probably as a result of the modification of pH and redox potential under

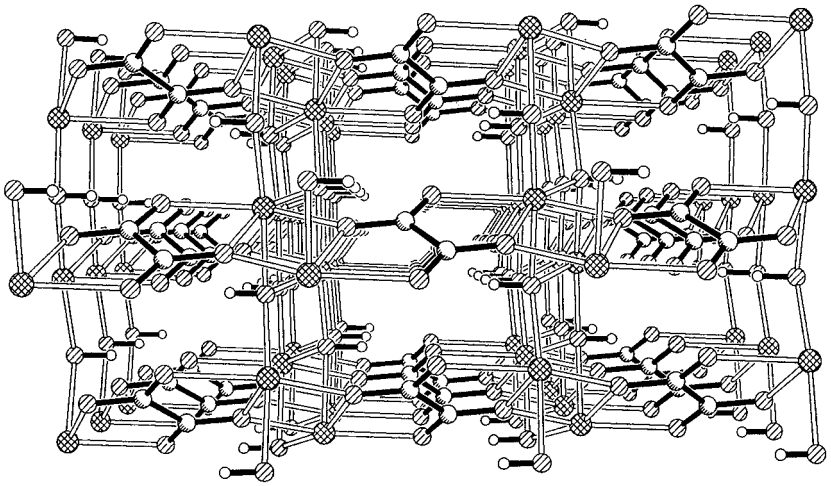

Figure 12. Packing diagram of $M_2(OH)_2(ox)$ showing the two-dimensional character of the M(OH) layers held apart by oxalato anions.

hydrothermal conditions (Molinier *et al.* 1997). It was found that using iron(II) starting materials only led to the formation of the mineral humboldtine, $Fe(ox)(H_2O)_2$, or other iron(II) minerals such as siderite, $FeCO_3$. The corresponding cobalt(II) compound, $Co_2(OH)_2(ox)$, is prepared from cobalt(II) starting materials without difficulty. $Co_2(OH)_2(ox)$ and $Fe_2(OH)_2(ox)$ are isostructural with layers of metal hydroxide connected by oxalate anions (figure 12). The metal hydroxide layers adopt a structure related to that of brucite (figure 1), except that pairs of μ_3-OH bridges are replaced by oxygen atoms from the oxalate ligands (figure 13) and the overall framework is distorted from the idealized triangular lattice of brucite (figure 14).

The magnetic behaviour of both compounds reflects this change in spin topology through the introduction of defects and distortion to the brucite structure. For the iron(II) compound, the plot of magnetization versus temperature is complicated by the presence of tiny amounts of magnetite, which are always present in the synthesis of this material. The fact that the curve is only displaced by about 11 G cm^3 mol^{-1} indicates that this impurity is at a very low level. Looking at the shape of the curve, we can identify two cusps at 120 K and 90 K and the onset of a spontaneous magnetization at 12 K (figure 15). The first and largest cusp at 120 K is due to the Vewery transition in the ferrimagnetic magnetite impurity (see, for example, Chikazumi 1964), but the second cusp at 90 K marks the onset of antiferromagnetic ordering in $Fe_2(OH)_2(ox)$. On further cooling, the rapid increase in magnetization at 12 K is indicative of spontaneous magnetization, but the absolute value attained is only a tiny fraction of what would be expected for a parallel, ferromagnetic arrangement. The comparison with the situation for the cobalt(II) compound (figure 15) shows, qualitatively, the same thermally dependent features. In this case, there is a single cusp reaching a maximum at 84 K with the onset of spontaneous magnetization at 32 K. Again, the absolute value of this magnetization is much smaller than would be expected for a parallel spin arrangement. The qualitative similarities of the magnetic behaviour of the Fe(II) and Co(II) systems allow us to suggest the following interpretation of the magnetism for both by analysing the data for the Co(II) system further.

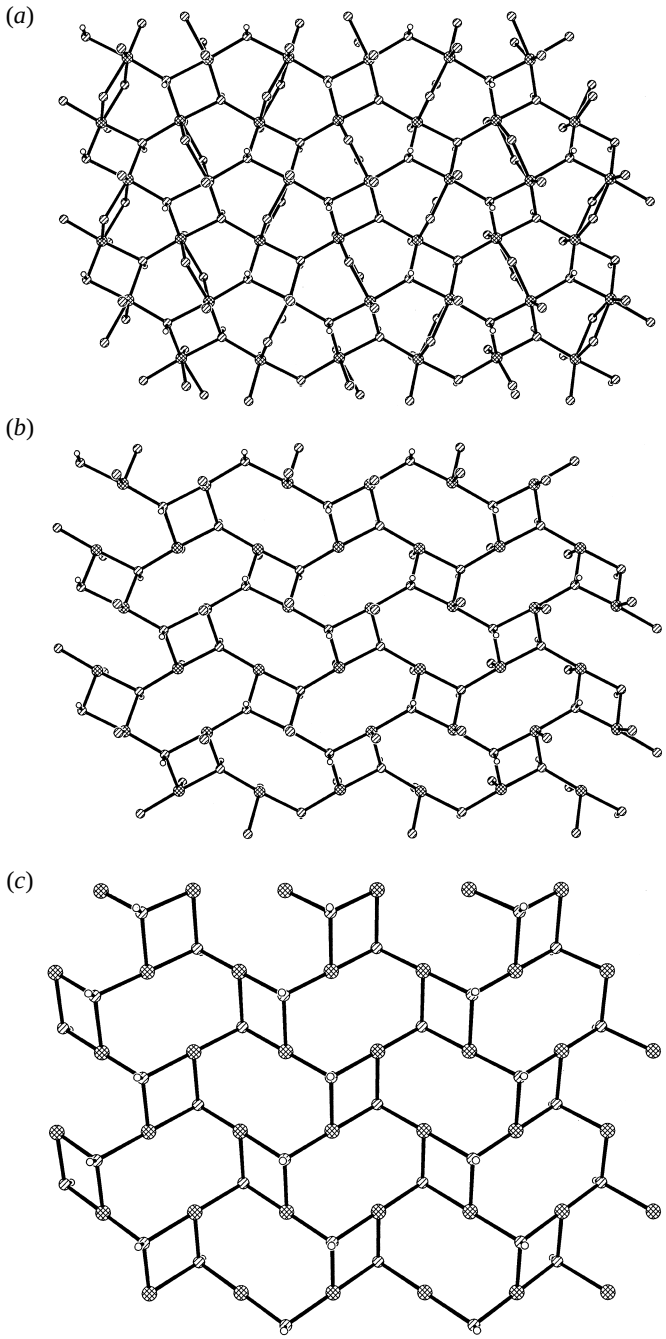

Figure 13. (*a*) Layer of $M_2(OH)_2(ox)$ showing how metal atoms are bridged by μ_3-hydroxide and μ_2 bridging oxalate oxygen atoms. (*b*) The same layer showing the hydroxy bridging only. (*c*) The equivalent structure formed by removing selected pairs of bridging hydroxides from the brucite lattice.

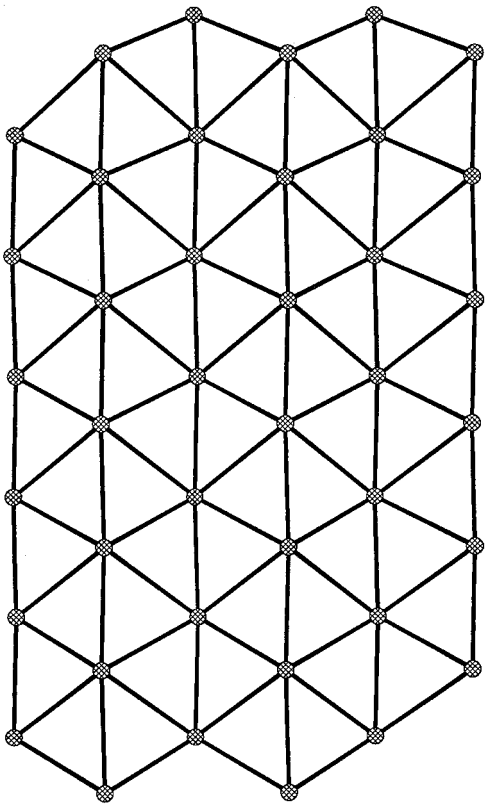

Figure 14. The distorted triangular net formed by a layer of the spin carrying metal ions in $M_2(OH)_2(ox)$. The bonds represent nearest-neighbour interactions for which at least one single bridging atom superexchange pathway exists.

The plot of reciprocal susceptibility versus temperature for $Co_2(OH)_2(ox)$ (figure 16) in the paramagnetic region (above 84 K) follows a Curie–Weiss law and can be extrapolated to give a negative intercept of $\vartheta = -117$ K, supporting the suggestion that there is a dominant antiferromagnetic interaction. This, coupled with the small absolute values for the spontaneous magnetization observed in the low temperature phase, leads to the conclusion that antiferromagnetically ordered spin canting is responsible for this. We can understand the antiferromagnetic ordering from the details of the single crystal X-ray structure analysis (Gutschke *et al.* 1999*a*), which shows that within a given layer of the structure there are six Co(II) neighbours linked through single-atom superexchange pathways at distances ranging between 3.18 and 3.69 Å. Four of these neighbours are linked by single μ_3-hydroxide oxygen atoms, a fifth is linked by two such μ_3-hydroxide oxygen atoms, and the sixth by two μ_2-oxalate oxygen atoms. The magnetic ions in each layer are connected to magnetic ions of neighbouring layers *via trans* oxalate bridges, giving a three-atom superexchange pathway and placing the metal ions from adjoining layers at 5.759(5) Å (figure 12). Although, from a structural point of view, we might expect the material to have a two-dimensional character, it is evident from the phase transition to an ordered antiferromagnetic state that there is significant exchange between layers.

From the Néel temperature, T_N, we can estimate an average exchange interaction,

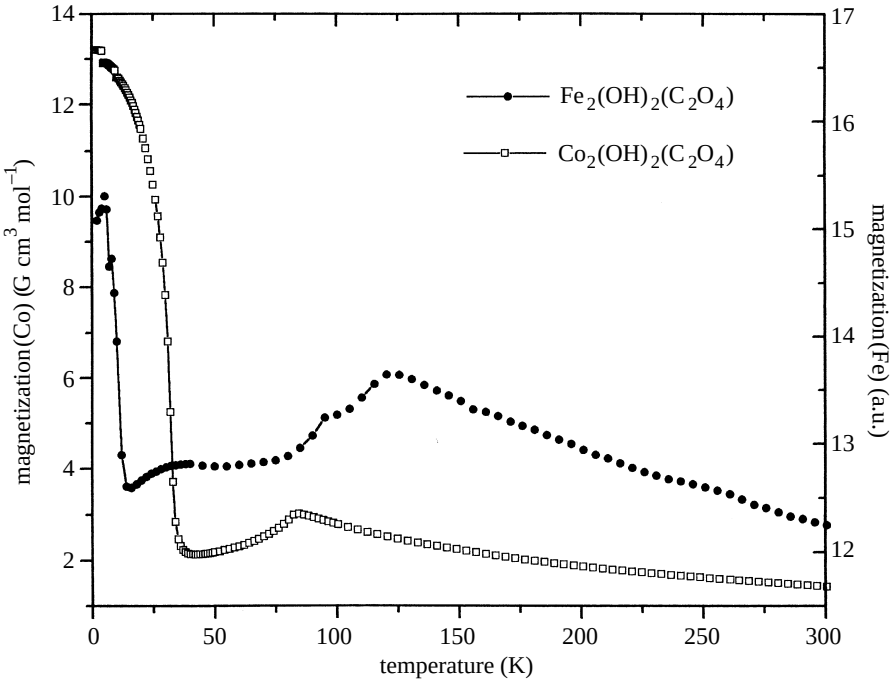

Figure 15. The temperature dependence of the magnetization curves for $Fe_2(OH)_2$(ox) and $Co_2(OH)_2$(ox). The displacement of the curve for $Fe_2(OH)_2$(ox) results from the small amount of magnetite impurity (see text).

J, of $-4.6\,\mathrm{cm}^{-1}$ using molecular field theory. This simplistic approach makes no distinction between intra- and interlayer couplings, so that, as in many other materials, the inadequacy of molecular field theory is revealed by the inequivalence of $|\vartheta|$ (117 K) and T_N (84 K).

A qualitative description of the situation can be used to help understand the magnetism of these $M_2(OH)_2$(ox) phases. The transition from a paramagnetic state to one of long-range order for a given structure is determined principally by the strength of spin–spin interactions, namely, the coupling, J. Since T_N for the Fe(II) compound is greater than T_N for the Co(II) compound (90 K versus 84 K), the absolute value of J for the Fe(II) must be somewhat greater than that for Co(II) and also more negative as a result of stronger antiferromagnetic coupling. On the other hand, the onset of canted antiferromagnetic behaviour requires not only an exchange coupling term, but also a term favouring a non-collinear spin configuration. This can be due to non-collinear single-ion anisotropies or to an antisymmetric exchange term. Both mechanisms will contribute to an energy term, D, favouring a non-collinear spin arrangement. If D were much larger than J, then we would expect the transition from paramagnet to canted antiferromagnet to occur directly, without the appearance of the intermediate antiferromagnetic phase as the temperature is decreased (Gutschke *et al.* 1999*b*). Conversely, if D is much smaller than J, then we would expect to see the phase transition sequence on cooling follow the order observed here: paramagnet, antiferromagnet, canted antiferromagnet. Thus, we can assign a larger absolute value for J than for D. Furthermore, since the onset of the spin-canted

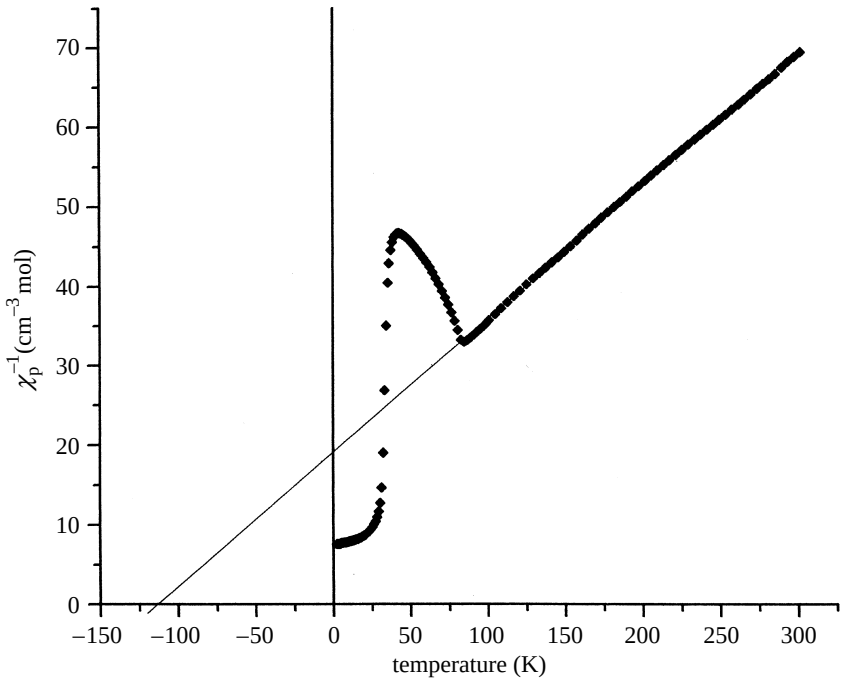

Figure 16. Reciprocal susceptibility as a function of temperature for $Co_2(OH)_2(ox)$ showing the good fit of the data in the paramagnetic region above 84 K to Curie–Weiss behaviour. The large negative intercept on the ordinate corresponds to the Weiss constant, θ, of −117 K.

phase occurs at a higher temperature for the Co(II) system than for the Fe(II) one, we can also assign a larger absolute value of D for the Co(II) case.

Spin canting can be described phenomenologically by a term $\boldsymbol{d} \cdot \boldsymbol{S}_1 \times \boldsymbol{S}_2$ in the spin Hamiltonian. There are two distinct mechanisms by which such a term can stabilize a non-collinear spin arrangement, either through single-ion anisotropy or by antisymmetric exchange interactions (Moriya 1963; Carlin 1986). For any magnetic phase with a spontaneous magnetization, very stringent symmetry requirements must be met, namely, that the magnetic symmetry element $\bar{I}'$ must be absent from the magnetic space group of the phase. If this element is present there can be no net magnetization, thus, certain magnetic space groups are incompatible with ferromagnetic, ferrimagnetic and canted antiferromagnetic phases (Briss 1964; Joshua 1991; Opechowski & Guccione 1965). This incompatibility is easily understood, since the $\bar{I}'$ element relates two spin sites by a crystallographic inversion centre where the moments are aligned exactly antiparallel and spin magnetic moments strictly cancel. The magnetic phase transition is second order and, thus, the magnetic space group of a canted antiferromagnet and of the underlying antiferromagnetic structure must be the same. Hence, we need to find the simple antiferromagnetic structures for which $\bar{I}'$ is not a symmetry element.

$Fe_2(OH)_2$ox and $Co_2(OH)_2$ox are isomorphous and isostructural, crystallizing in the monoclinic space group $P2_1/c$. The four crystallographically equivalent metal ions generated by the symmetry elements of the $P2_1/c$ space group within the chemical unit cell each have seven near neighbours. However, only three independent

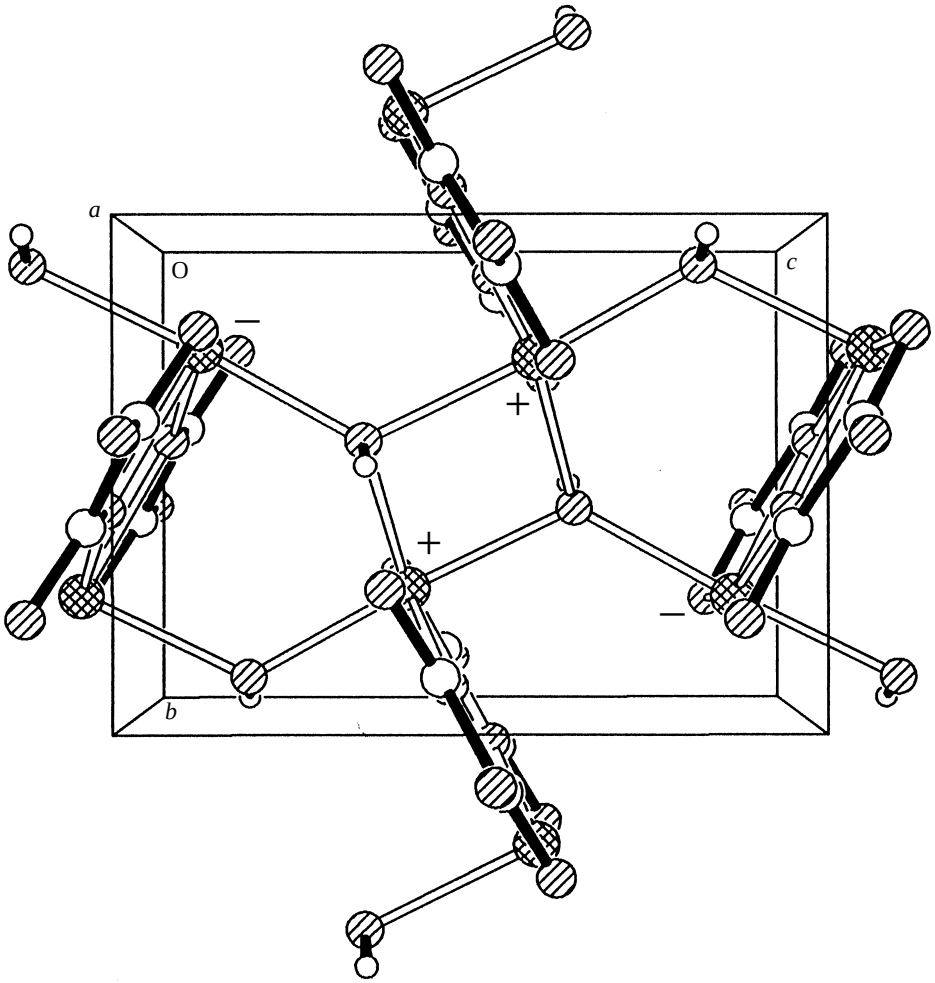

Figure 17. The proposed magnetic unit cell and spin configuration for the ordered antiferromagnetic states of $M_2(OH)_2(ox)$ (+ indicates spin-up, − indicates spin-down).

couplings are necessary to describe the spin arrangement throughout the crystal. For the most likely arrangement of the spins according to a simple two-sublattice model, there are eight possible different spin configurations for the three principal couplings relating parallel (ferromagnetically coupled) or antiparallel (antiferromagnetically coupled) moments. Four of these correspond to magnetic unit cells that are the same size as the crystallographic chemical unit cells, with the other four corresponding to magnetic unit cells that are doubled along the a-axis. The magnetic space groups for each of these eight spin configurations were determined for many orientations of the spin vectors (e.g. with the sublattice magnetizations parallel to the lattice vectors $\boldsymbol{a}$, $\boldsymbol{ab}$, $\boldsymbol{b}$, $\boldsymbol{bc}$, $\boldsymbol{c}$, $\boldsymbol{ac}$ and $\boldsymbol{abc}$). Only one spin configuration (figure 17) corresponded to a set of magnetic space groups for which the $\bar{I}'$ element was absent. These were $P2_1/c$ for the sublattice magnetizations parallel to the b-axis, $P2_1'/c'$ if the spin vectors are confined to the ac-plane, and $P\bar{I}$ otherwise.

Neutron diffraction studies are planned to confirm the spin configurations and to determine the orientation of the Néel vector in the hydroxyoxalate phases. It is interesting that the very stringent requirements of canted antiferromagnetism have, in this case, enabled us to determine the probable spin configuration of the canted and antiferromagnetic phases from logical symmetry considerations. Although, to a first approximation, these materials are topologically stacked triangular lattices, the geometric distortion and consequent reduction in symmetry causes a simplification of the magnetic phase behaviour compared with the related binary divalent transition-metal hydroxides and halides (Day 1988; Aruga Katori *et al.* 1996; de Jongh 1990). We have reported elsewhere that when the hydrothermal syntheses that produce $Fe_2(OH)_2(ox)$ are allowed to proceed further or with slightly altered reaction protocols (Molinier *et al.* 1997), then the iron oxide phases of magnetite and haematite can result. Indeed, we found that the magnetite we observed displayed rhombic dodecahedral crystal morphology rather than the more usual octahedral or cubic ones. We were able to show that this was probably the result of the inclusion of the oxalate template in the $Fe_2(OH)_2(ox)$ precursor acting as a growth inhibitor. From this, we can gain insights into the way in which templating species can direct the form and function of extended phases.

4. Conclusions

The two types of system reported here represent two ways of manipulating the brucite lattice to give materials with interesting magnetic properties. The Fe_{17}/Fe_{19} aggregates, which trap small portions of the brucite lattice, prove not only to be useful structural 'scale' models for the protein ferritin, but also display magnetic phenomena that could help in the interpretation of the magnetic behaviour observed for ferritins. The second system, $M_2(OH)_2(ox)$, reveals how the introduction of defects into the extended brucite structure alters the magnetic behaviour through the distortion of the simple triangular lattice.

Thus, we have shown how the introduction of templating species can be used to manipulate a simple hydroxide structure in order to produce materials with magnetic properties significantly different from those of the parent lattice in a manner akin to that used in nature in the process of biomineralization.

We thank Wolfgang Wensdorfer for performing the microSQUID measurements and the EPSRC and Wellcome Trust for funding.

References

Aruga Katori, H., Katsumata, K. & Katori, M. 1996 *Phys. Rev.* B **54**, R9620.

Awschalom, D. D., Smyth, J. F., Grinstein, G., DiVincenzo, D. P. & Loss, D. 1992 *Phys. Rev. Lett.* **68**, 3092.

Baissa, E., Mandel, A., Anson, C. E. & Powell, A. K. 1999 Single crystal X-ray diffraction reveals supramolecular interactions between novel Al_{15} clusters to produce zeotypiclattices. (In preparation.)

Briss, R. R. 1964 *Symmetry and magnetism, selected topics in solid state physics* (ed. E. P. Wohlfarth). Amsterdam: North Holland.

Carlin, R. L. 1986 *Magnetochemistry*. Springer.

Cheesman, M. R., Oganesyan, V. S., Sessoli, R., Gatteschi, D. & Thomson, A. J. 1997 *Chem. Commun.*, p. 1677.

Chikazumi, S. 1964 *Physics of magnetism*, p. 387. Wiley.

Chudvonsky, E. M. 1996 *Science* **274**, 938.

Cornell, R. M. & Schwertmann, U. 1996 *The iron oxides*. Weinheim: VCH.

Day, P. 1988 *Acc. Chem. Res.* **21**, 250.

de Jongh, L. J. (ed.) 1990 *Magnetic properties of layered transition metal compounds*. Dordrecht: Kluwer.

Dormann, J. L., Bessais, L. & Fiorani, D. 1988 *J. Phys.* C **21**, 2015.

Ford, G. C., Harrison, P. M., Rice, D. W., Smith, J. M. A., Treffry, A., White, J. L. & Yariv, J. 1984 *Phil. Trans. R. Soc. Lond.* B **304**, 551.

Frankel, R. B. & Blakemore, R. P. (eds) 1990 *Iron biominerals*. New York: Plenum.

Friedman, J. R., Sarachik, M. P., Tejada, J. & Ziolo, R. 1996 *Phys. Rev. Lett.* **76**, 3830.

Gatteschi, D., Canneschi, A., Pardi, L. & Sessoli, R. 1994 *Science* **265**, 1054.

Gutschke, S. O. H., Price, D. J., Powell, A. K. & Wood, P. T. 1999*a* Synthesis, single crystal X-ray structure and properties of CO_2 $(OH)_2$ (OX). (In preparation.)

Gutschke, S. O. H., Price, D. J., Powell, A. K. & Wood, P. T. 1999*b* *Angew. Chem. Int. Ed. Engl.* **38**, 1088.

Heath, S. L. 1992 PhD thesis, University of East Anglia, Norwich.

Heath, S. L. & Powell, A. K. 1992 *Angew. Chem. Int.* **31**, 191.

Heath, S. L., Jordan, P. A., Johnson, I. D., Moore, G. R., Powell, A. K. & Helliwell, M. 1995 *J. Inorg. Biochem.* **59**, 785.

Heath, S. L., Charnock, J. M., Garner, C. D. & Powell, A. K. 1996 *Chem. Eur. J.* **2**, 634.

Joshua, S. J. 1991 *Symmetry principles and magnetic symmetry in solid state physics*. Bristol: Adam Hilger.

Kahn, O. 1993 *Molecular magnetism*. Weinheim: VCH.

Le Brun, N. E., Thomson, A. J. & Moore, G. R. 1997 *Struct. Bonding* **88**, 103.

Mann, S., Webb, J. & Williams, R. J. P. (eds) 1989 *Biomineralization*. Weinheim: VCH.

Molinier, M., Price, D. J., Wood, P. T. & Powell, A. K. 1997 *J. Chem. Soc. Dalton Trans.*, p. 4061.

Moriya, T. 1963 In *Magnetism* (ed. G. T. Rado & H. Suhl), vol. I, ch. 3, p. 85. Academic.

Opechowski, W. & Guccione, R. 1965 In *Magnetism* (ed. G. T. Rado & H. Suhl), vol. IIa, ch. 3, p. 105. Academic.

Powell, A. K. 1997 *Struct. Bonding* **88**, 1.

Powell, A. K., Heath, S. L., Gatteschi, D., Pardi, L., Sessoli, R., Spina, G., Del Giallo, F. & Pieralli, F. 1995 *J. Am. Chem. Soc.* **117**, 2491.

Russell, J. D. 1979 *Clay Miner.* **14**, 109.

Stamp, P. C. E. 1996 *Nature* **383**, 125.

Tejada, J. & Zhang, X. X. 1994 *J. Phys. Condens. Matter* **6**, 263.

Tejada, J., Ziolo, R. F. & Zhang, X. X. 1996 *Chem. Mater.* **8**, 1784.

Thomas, L., Lionti, F., Ballou, R., Gatteschi, D., Sessoli, R. & Barbara, B. 1996 *Nature* **383**, 145.

Towe, K. M. & Bradley, W. F. 1967 *J. Colloid Interface Sci.* **24**, 384.

Wells, A. F. 1962 *Structural inorganic chemistry*, 3rd edn. Oxford University Press.

Wernsdorfer, W. 1996 PhD thesis, Université Joseph Fourier, Grenoble, France.

Womack, T. G. 1999 PhD thesis, University of East Anglia, Norwich.